http://tandfonline.com/inan
ISSN: 1743-5390 (print), 1743-5404 (electronic)

Nanotoxicology

Nanotoxicology, 2016; 10(8): 1129–1135
 DOI: 10.1080/17435390.2016.1179809

Taylor & Francis
Taylor & Francis Group

ORIGINAL ARTICLE

Cellular internalization and intracellular biotransformation of silver nanoparticles in *Chlamydomonas reinhardtii*

Songshan Wang[1], Jitao Lv[1], Jingyuan Ma[2], and Shuzhen Zhang[1]

[1]*State Key Laboratory of Environmental Chemistry and Ecotoxicology, Research Center for Eco-Environmental Sciences, Chinese Academy of Sciences, Beijing, P.R. China and* [2]*Shanghai Synchrotron Radiation Facility, Shanghai Institute of Applied Physics, Chinese Academy of Sciences, Shanghai, P.R. China*

Abstract

It is necessary to elucidate cellular internalization and intracellular biotransformation in order to accurately assess the toxicity and fate of nanoparticles after interaction with organisms. Therefore, this work employed a combination of high resolution imaging and *in situ* detection spectroscopic techniques to systematically investigate the intracellular localization, morphology and chemical speciation of silver in the cells of *Chlamydomonas reinhardtii*, a unicellular freshwater green alga, after exposure to AgNPs coated with polyvinylpyrrolidone at a concentration of 2.0 mg/L. High resolution secondary ion mass spectrometry and high-angle annular dark field scanning transmission electron microscopy together with energy dispersive spectroscopy and selected area electron diffraction collectively confirmed that after 48 h of exposure, AgNPs entered the periplasmic space after cellular internalization into the algal cells. Silver was also found to coexist with sulfur inside the cytoplasm in both crystalline and amorphous forms, which were further identified as β-Ag_2S and silver thiolates with synchrotron X-ray absorption spectroscopy. In combination, these analyses demonstrated that silver inside algae could be attributed to the uptake and sequestration of Ag^+ ion released from AgNPs, which was further sequestrated into cellular compartments. This study provides solid evidence for particle internalization and biotransformation of AgNPs after interaction with algae.

Keywords

Chlamydomonas reinhardtii, HAADF-STEM, NanoSIMS, silver nanoparticles, XAS

History

Received 24 December 2015
Revised 14 March 2016
Accepted 11 April 2016
Published online 10 May 2016

Introduction

Silver nanoparticles (AgNPs) are widely used in numerous technologies and incorporated into a wide array of consumer products due to their antibacterial properties (Seltenrich, 2013; Tulve et al., 2015). AgNPs can be released into aquatic environments during manufacture, usage or disposal, with environmental concentrations estimated at the level of ng/L in surface water (Hedberg et al., 2014; Mitrano et al., 2014), and expected to continue increasing. The AgNPs released into the environment will inevitably interact with aquatic organisms, posing potential hazards to aquatic ecosystems. Therefore, there is a considerable effort underway to understand the environmental behaviors and toxicities of AgNPs in aquatic environments (Fabrega et al., 2011; Sharma et al., 2014).

Green algae lie at the lowest trophic level and constitute the basis of many aquatic food chains. Studies have demonstrated the toxicity of AgNPs toward the photosynthesis, growth and natural community structure of green algae and particular attention has been paid to distinguish the toxic effects derived from AgNPs and those from the Ag^+ ion released from AgNPs (Das et al., 2014; Navarro et al., 2015; Sorensen & Baun, 2015). The toxicity of AgNPs to algae is expected to be determined by their uptake and accumulation in cells. However, it is still unclear whether there is cellular internalization of AgNPs in algae. The cell wall and membrane of green algae form barriers that impede cellular internalization of exogenous substances. Penetration through pores in the cell wall and transport across the membrane via endocytosis or passive diffusion have been proposed to be the most feasible routes for cellular internalization of AgNPs by algae (Behra et al., 2013; von Moos et al., 2014). However, there is a lack of sufficient evidence to support such speculation, and contradictory results have been obtained from the limited observations on the uptake of AgNPs by algae, with some researchers asserting cellular internalization of AgNPs but others not (Leclerc & Wilkinson, 2014; Miao et al., 2010; Ribeiro et al., 2015).

In situ identification and localization of nanoparticles in cells remain as challenges for many kinds of nanoparticles such as AgNPs. Bright field transmission electron microscopy (BF-TEM) has been most frequently applied to observe the accumulation of AgNPs in cells due to its ultrahigh 2D resolution (Thorley et al., 2014; Yang et al., 2014). However, electron-dense substances that develop during sample preparation or algal growth create difficulties for the observation of AgNPs in algae (Hong-Hermesdorf et al., 2014). Techniques such as dark field microscopy coupled with hyperspectral imagery (Pratsinis et al., 2013), focused ion beam scanning electron microscopy (FIB-SEM) (Garcia et al., 2014), coherent anti-stokes Raman scattering (CARS) microscopy (Ribeiro et al., 2015) and synchrotron radiation based transmission X-ray microscopy (SR-TXM) (Wang et al., 2015) have been explored in recent years to directly

Correspondence: Shuzhen Zhang, Research Center for Eco-Environmental Sciences, Chinese Academy of Sciences, 18 Shuangqing Road, Haidian District, 100085 Beijing, P.R. China. Tel: +86 1062849683. Fax: +86 1062923563. E-mail: szzhang@rcees.ac.cn

observe AgNPs in cells. Nevertheless, the limited sensitivity or spatial resolution and uncertainty of Ag speciation make them insufficient to confirm or exclude cellular internalization of AgNPs, particularly in the case when only one of the techniques is employed. Therefore, a combination of high-resolution techniques is believed to be an important approach to address the issues of cellular internalization and biotransformation of AgNPs.

Moreover, AgNPs are prone to undergo chemical transformation, which may accompany the process of cellular internalization of AgNPs by algae and affect their uptake and accumulation. Chemical transformation of AgNPs has drawn much attention (Levard et al., 2012), but most of the research has focused on their environmental transformation. The results of related studies suggest that AgNPs are subject to oxidative dissolution and reactions with reduced sulfur species, chloride and organic ligands in aquatic environments (Chen et al., 2013b; Liu et al., 2012; Lowry et al., 2012; Sekine et al., 2013; Wang et al., 2014). In comparison, less is known about transformation of AgNPs in biological organisms. Biotransformation of AgNPs in mammal cells and in killifish embryos has been investigated recently, and transformation products were identified as complexes with functional groups containing O or S in proteins or peptides (Auffan et al., 2014; Chen et al., 2013a; Cronholm et al., 2013; Hsiao et al., 2015; Jimenez-Lamana et al., 2014). Nevertheless, such observations have only been made through *in vitro* experiments with cell cultures, and *in vivo* evidence is lacking. Moreover, to date there is no clear understanding of how intracellular biotransformation of AgNPs occurs in cells such as green algal cells, which is essential to determine the toxicological mechanisms and ultimate risks of AgNPs in the aquatic environment.

High resolution secondary ion mass spectrometry (NanoSIMS) is a nanoscale ion microprobe and offers a spatial resolution down to 50 nm with high elemental sensitivity, making it one of the most powerful tools to quantitatively investigate elemental distribution in organisms at the cellular level (Moore et al., 2014). High-angle annular dark field scanning transmission electron microscopy (HAADF-STEM) is suitable for distinguishing elements with high atomic number, such as Ag, from the major elements in living organisms such as C, N and O, with a high spatial resolution (~1 nm) (Kim et al., 2010). Therefore, an attempt was made in the present study to employ a combination of NanoSIMS and HAADF-STEM together with energy dispersive spectroscopy (EDS), selected area electron diffraction (SAED) and *in situ* synchrotron X-ray absorption spectroscopy (XAS) detection to systematically investigate the intracellular localization, morphology and chemical speciation of Ag within the cells of *Chlamydomonas reinhardtii* (a unicellular freshwater green alga) after exposure to AgNPs, in comparison with ionic silver (Ag^+). The purpose of this study was to uncover whether cellular internalization and intracellular biotransformation of AgNPs in *C. reinhardtii* occurred and what the relevant mechanisms may be.

Experimental section

Strain and cultivation

Chlamydomonas reinhardtii (FACHB-1121, wild type) was obtained from the Freshwater Algae Culture Collection at the Institute of Hydrobiology, Chinese Academy of Sciences. The alga was single-colony purified and transferred from the initial Bristol's solution to a Tris–acetate–phosphate (pH 7.0, ionic strength 0.03 M) medium under constant agitation and illumination of 2000 lux at 25 °C (Harris, 2009). Ammonium acetate was substituted for ammonium chloride in the medium to avoid the precipitation of AgCl. A hemocytometer was used to estimate the cell density of the culture applied to exposure experiments. The medium after alga cultivation was precipitated with 80% ethanol to obtain the algal extracellular polymeric substances.

Preparation and characterization of AgNPs

The AgNPs were prepared via a liquid reduction method. Briefly, a 200-mL aqueous solution containing silver nitrate (50 mM, 1.0 mL) and polyvinylpyrrolidone (50 mM, 1.0 mL, TCI K15) was vigorously stirred at room temperature. Freshly prepared ice-cold sodium borohydride (0.6 mL, 100 mM) was immediately injected into the mixed solution. The solution was filtered through a 0.22-μm cellulose acetate membrane after 2 h of stirring. An Ultracel 3 K Centrifugal Filter Device (Amicon Millipore, Darmstadt, Germany) with a molecular cutoff of 3 kDa was utilized to concentrate the AgNP solution and remove excessive ions by rinsing with Milli-Q water (18.2 MΩ·cm at 25 °C) three times. The concentrated solution was centrifuged at 5000*g* for 40 min and deoxygenated under pure nitrogen flow to obtain the AgNP stock solution, and then kept at 4 °C before use.

Concentrations of total silver and dissolved Ag^+ ion in the AgNP stock solution were analyzed by an inductively coupled plasma optical emission spectrometer (ICP-OES, Optima 8300, PerkinElmer, Waltham, Massachusetts). The stock solution was subjected to ultrafiltration with a 3 kDa membrane and the concentration of dissolved Ag^+ ion was determined. The zeta potential of the AgNPs was measured by electrophoretic mobility using a Zetasizer (Nano ZS, Malvern Instruments, Worcestershire, UK). Measurement of surface plasmon resonances was carried out on a Shimadzu UV-visible spectrophotometer (UV-2550, Tokyo, Japan). The size of the AgNPs was characterized using transmission electron microscopy (TEM, H-9000NAR, Hitachi, Tokyo, Japan) on a carbon-coated copper grid.

Exposure experiments

After being grown until a mid-log phase (within 48–72 h of inoculum culture), algae were collected by centrifugation at 4000*g* for 2 min, and then diluted with fresh medium to 10 mL in a 25-mL glass flask to reach a final cell density of $0.6–0.8 \times 10^6$ cells/mL. After 24 h of cultivation, stock solutions of AgNPs or Ag^+ (supplied as silver nitrate) were added to achieve the final Ag concentration of 2.0 mg/L for AgNPs and 0.30 mg/L for Ag^+, respectively. All treatments were conducted in triplicate. Algae were harvested by 4000*g* centrifugation for 2 min at the time intervals of 4, 12, 24, 36 and 48 h, respectively. The algal pellet was washed three times with fresh medium. The silver concentration in the algal pellet and supernatant was determined by inductively coupled plasma mass spectrometry (ICP-MS, Agilent 8800, Agilent Technologies, Santa Clara, CA) after digestion with concentrated nitric acid.

Sample preparation for spectroscopic analysis

Algae were harvested by centrifugation after 48 h of exposure to 2.0 mg/L AgNPs or 0.3 mg/L Ag^+. The algal pellet was pre-fixed with 2.5% glutaraldehyde in 0.1 mol/L cacodylic acid buffer (pH of 7.2) at 4 °C overnight and then washed three times with pre-chilled cacodylic acid buffer. Subsequently, the algal pellet was subject to post-fixing with 1% osmic acid in 0.1 mol/L cacodylic acid buffer and washed with cacodylic acid buffer three times. Then, the pellet underwent gradient dehydration with 30%, 50%, 70%, 90% ethanol, 90% ethanol–90% acetone (1:1 v:v), 90% acetone and 100% acetone for 15 min, respectively. The sample was then embedded in Quetol 812 epoxy resin (Nisshin EM, Tokyo, Japan) and polymerized according to the following schedule: 37 °C for 12 h, 45 °C for 12 and then 60 °C for 24 h. An ultramicrotome (Reichert OM U2, Depew, NY) was used to

slice the resin-fixed sample into thin sections for HAADF-STEM and NanoSIMS analysis.

Electron microscopy

The algal pellet after pre-fixation was directly subjected to gradient dehydration without osmic acid post-fixation. Sample slices with a thickness of 70 nm were deposited on a carbon support film on a 230 mesh copper grid and observed with a FEI Tecnai F20, Hillsboro, Oregon or JEOL JEM-2010F, Tokyo, Japan transmission electron microscope at 200 keV accelerating voltage. The image was captured in HAADF-STEM mode. EDS spot and mapping analysis and SAED were performed to analyze the regions of interest. SAED was undertaken in BF-TEM mode.

NanoSIMS

Sample slices with a thickness of 400 nm were deposited onto a steel cylinder (10 mm in diameter) and analyzed with a NanoSIMS 50 (Cameca, Gennevilliers, France) using a Cs^+ primary source (8 keV). Images were acquired with a dwell time of 10 ms at a size of $20 \times 20\ \mu m^2$ and 256×256 pixels. The masses detected simultaneously in multi-collection mode were $^{12}C^{14}N^-$ (m: 26.00307), $^{32}S^-$ (m: 31.97207), $^{107}Ag^-$ (m: 106.90486) and $^{109}Ag^-$ (m: 108.90575), respectively. The data were analyzed using ImageJ with the OpenMIMS plugin (Harvard, Cambridge, MA).

Synchrotron X-ray absorption spectrum analysis

One hundred milliliters of the culture mixture was centrifuged at 20 000*g* for 40 min after exposure to 2.0 mg/L AgNPs for 24 and 72 h, respectively. The silver concentration in the supernatant was negligible according to analysis by ICP-MS. The pellet was pressed into slices using a tablet pressing machine at 1 MPa pressure for 10 min after lyophilization. The slices were pasted on Kapton tape (3 M, St. Paul, MN) and then subjected to synchrotron-based XAS analysis at the 14 W beamline of the Shanghai Synchrotron Radiation Facility. Silver (25 514 eV) K-edge XAS spectra were collected in an energy range of −200 to 800 eV from the absorption edge. A silver-ion-adsorbed alga sample was prepared by adding 100 mL of silver nitrate (50 mg/L) to the harvested algal pellet and then shaking at room temperature for 24 h. Reference materials for XAS data analysis included AgNPs (Ag^0), silver oxide (Ag_2O), silver chloride (AgCl), silver sulfate (Ag_2SO_4), silver phosphate (Ag_3PO_4), silver nitrate ($AgNO_3$), silver citrate ($C_6H_5Ag_3O_7$), silver sulfide (Ag_2S), silver diethyldithiocarbamate ($(C_2H_5)_2NCSAg$), silver glutathione complexes (Ag-GSH) and glutathione (γ-Glu-Cys-Gly) to represent phytochelatins (γ-(Glu-Cys)n-Gly). The XAS spectra of the reference materials were collected in transmission mode, while those of the samples were collected in fluorescence mode.

The IFEFFIT (version 1.2.10) package was used for the analysis of XAS spectra. Linear combination fitting (LCF) of XANES data for the AgNP-exposed algal samples was performed in the range of −30 to +50 eV below and above the Ag K-edge (25 514 eV). Levenberg–Marquardt nonlinear least square fitting of EXAFS data was performed for all the reference materials and samples.

Results

Characterization of AgNPs

The extinction spectra of AgNPs peaked at 395 nm, with a full width at half maximum of 49 nm (Figure S1a in the Supporting Information). The particle size obtained from TEM image analysis ranged from 7 nm to 17 nm with an average of 11.7 ± 1.9 nm (Figures S1b and S1c). The zeta potential of AgNPs was significantly lower in the medium containing 10 mg C/L of algal extracellular polymeric substance (EPS) (-25 ± 0.2 mV, pH 7.0) than in the pure TAP medium (-21 ± 1.0 mV, pH 7.0, $p < 0.01$). Dissolved Ag^+ ion accounted for approximately 0.44% of the total Ag in the stock solution.

Uptake of silver by the algae exposed to AgNPs and Ag^+

AgNPs and Ag^+ at the employed exposure concentrations caused no significant toxic effects to the algae after exposure for 48 h, and algal biomass was comparable between the two exposures (Figure S2). There was no obvious precipitation or loss of AgNPs during algal growth and harvesting (see details in the Supporting Information). Bioaccumulation of Ag in the algae conformed to first-order kinetics and reached an apparent equilibrium at 48 h, with concentrations of 1761 and 233 mg/L_{cell} for the exposures to AgNPs and Ag^+, respectively (Figure 1).

Distribution and characterization of silver in the algae

NanoSIMS was applied for the first time to analyze the distribution of Ag together with C, N and S in the algal cells. The measured $^{109}Ag^-/^{107}Ag^-$ ratio coincided with the terrestrial Ag isotopic ratio, indicating that there was no mass interference (Figure S3). Ion maps of $^{107}Ag^-$, $^{12}C^{14}N^-$ and $^{32}S^-$ are presented in Figure 2. The control algae only showed very weak signals as noise in the $^{107}Ag^-$ image, and their occurrence had no correlation to the location of algal cells; whereas silver was observed to accumulate predominantly on the cell walls and in the cytoplasm of the algae after exposure to AgNPs and Ag^+. Comparatively, the intensity of $^{107}Ag^-$ on the cell wall was stronger for the exposure to AgNPs than for Ag^+ exposure. Bright

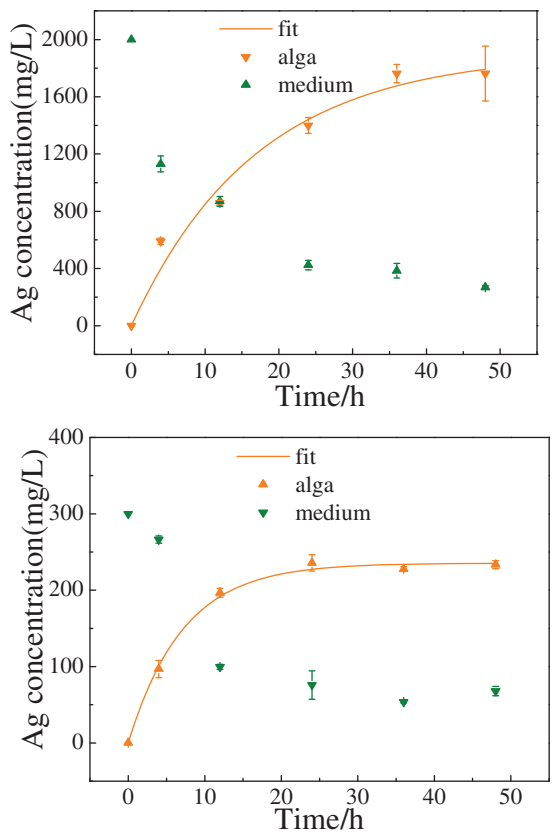

Figure 1. Uptake of silver in *C. reinhardtii* after exposure to AgNPs (upper) and Ag^+ (down) as a function of exposure time. The solid triangles and lines represent the experimental data with standard deviations and the first-order kinetic fittings, respectively.

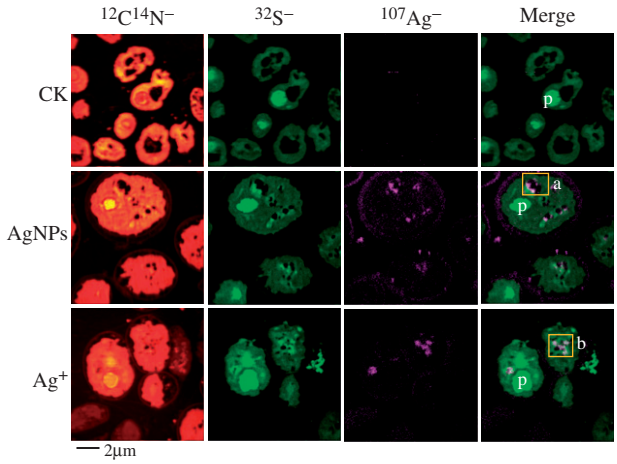

Figure 2. High-resolution secondary ion mass spectrometry (NanoSIMS) images showing the elemental distribution of $^{12}C^{14}N^-$, $^{32}S^-$ and $^{107}Ag^-$ in *C. reinhardtii*. The last images are the overlap of C, N, S and Ag images. p: pyrenoid.

spots existed in the cytoplasm for both exposures and on the cell walls only for the exposure to AgNPs, which might arise from AgNPs or their aggregates. Merging the images showed that there was no apparent overlap between the images of $^{32}S^-$ and $^{107}Ag^-$ on the cell walls of the algae after exposure to AgNPs. However, they overlapped each other in the cytoplasm for both AgNPs and Ag^+ exposures (areas a and b in Figure 2), suggesting co-accumulation of Ag and S in the cytoplasm. Accumulation of S was also high inside the pyrenoid due to the fact that it serves as a protein pool in cells, but there was no significant Ag accumulation.

HAADF-STEM was performed to explore the accurate location and morphology of Ag observed with NanoSIMS. The HAADF image of the control algae showed a weak contrast throughout the cell (Figure 3a), while the algae exposed to AgNPs or Ag^+ consisted of a set of bright spots located mainly in the periplasmic space (area a in Figure 3b and area c in Figure 3c) and cytoplasm (area b in Figure 3b and area d in Figure 3c). For the exposure to AgNPs, the BF-TEM images showed that the bright spots in the periplasmic space (Figure 3d) had a clear outline with diameter of approximately 10-20 nm (Figure 3e), surrounded by a considerable amount of relatively dark spots with diameter of 1-2 nm (Figures S4a and S4b). The bright spots in the cytoplasm were isolated within cellular compartments (Figure 3f), of which some were relatively bright with a clearly particulate appearance (area e in Figure 3g) and diameter of 10-20 nm (BF-TEM image in Figure 3h). The others appeared as a dense collection of tiny dark dots (area f in Figures 3g and 3i), which could not be recognized by the BF-TEM image (Figure S4c), and therefore should be substances in amorphous form. A similar observation was found in the periplasmic space and cytoplasm of the algae after exposure to Ag^+ (Figures 3j and 3k).

EDS analysis was carried out to identify the chemical compositions of the bright spots observed with HAADF in the algae. The characteristic peak of Ag $L_{\alpha 1}$ and $L_{\beta 1}$ in the EDS spectra confirmed that the bright spots were Ag-containing substances (Figure S5). For the bright spots in the periplasmic space, the characteristic peak of S $K_{\alpha 1}$ was very weak and rather inconsiderable compared with that of Ag (Figures S5a and S5b). For the bright spots in the cytoplasm, the characteristic $K_{\alpha 1}$ peaks of Ag and S always occurred concomitantly (Figures S5d–S5f). The atomic ratios of Ag to S were further calculated as 2:1 and 2.6:1 for the exposures to AgNPs and Ag^+, respectively (Figures S5d and S5f), equal or close to their ratio in Ag_2S, while the Ag/S value was 1.4:1 for the amorphous-form substances observed with HAADF-STEM as a dense collection of tiny dark dots (Figure S5e). EDS-mapping was further carried out to assess the coincidence of S with Ag in the area where Ag appeared in the algae. Consistent with the NanoSIMS images, only a tiny part of the Ag signals overlapped with those of S in the periplasmic space (Figure S6a), whereas Ag was found almost exclusively co-localized with S in the cytoplasm of algae after exposure to AgNPs and Ag^+ (Figures S6b and S6c). Therefore, it was quite likely that Ag co-accumulated with S in the cytoplasm but not in the periplasmic space.

Furthermore, SAED was performed to analyze the structural characteristics of the Ag-containing particles in the algae. For the particles in the periplasmic space of the algae after exposure to AgNPs, the SAED patterns revealed that a lattice plane with interplanar spacing of approximately 2.4 Å had the strongest diffraction intensity, followed by those with 2.0 and 1.2 Å spacings (inset in Figure 3b), which were consistent with the SAED patterns of {111}, {200} and {311} planes (lying in zone $[01\bar{1}]$) of face-centered cubic metallic Ag (Wyckoff, 1963). However, for the particles in the cytoplasm, the SAED patterns revealed comparable diffraction intensities for lattice planes with interplanar spacings of 2.4 and 2.0 Å and relatively weak intensity for the lattice plane of 1.4 Å (inset in Figure 3g), which was consistent with the SAED patterns of {013}, $\{20\bar{2}\}$ and {211} planes (lying in zone $[\bar{1}3\bar{1}]$) of β-Ag_2S (Sadanaga & Sueno, 1967). However, some impurities coexisted with β-Ag_2S, since none of the potential lattice planes in β-Ag_2S lying in the zone $[\bar{1}3\bar{1}]$) would generate electron diffraction at 1.2 Å. For the exposure to Ag^+, the SAED patterns of the particles in the periplasmic space revealed three planes with similar interplanar spacing in the range of 2.2–2.4 Å (inset in Figure 3j). Although it was difficult to identify the actual crystal phases, it was certain that they were not silver crystal or β-Ag_2S. Similar to the case for exposure to AgNPs, β-Ag_2S was identified for the particles in the cytoplasm, but without a diffraction spot deriving from the plane with interplanar spacing of 1.2 Å (inset in Figure 3k).

Speciation analysis of Ag by synchrotron XAS

Synchrotron-based Ag K-edge XAS was performed to distinguish Ag speciation before and after exposure for 24 and 72 h, respectively. The spectra were only collected for algae after exposure to AgNPs because the low exposure level of Ag^+ limited the collection of high-quality spectra. The height of the Ag^0 diagnostic peak in the range of 25 540–25 560 eV attenuated with the increase of exposure time (Figure 4a). Quantification analysis of the component percentage of Ag speciation was performed by LCF of the XANES spectra using the reference materials together with the Ag^+-adsorbed algal sample, and their spectra are provided in Figure S7. The XANES spectra together with fitting lines are shown in Figure 4a and the fitting results are provided in Figure S8, respectively. After exposure for 24 h, $62 \pm 1.7\%$ of Ag was present as Ag^0, followed by silver glutathione complexes and then Ag_2O. After exposure for 72 h, the percentage of Ag^0 dropped to $15 \pm 1.0\%$ and Ag_2O disappeared, whereas Ag glutathione complexes represented the dominant speciation ($51 \pm 2.4\%$) with Ag_2S as the remainder (Figure S8). The EXAFS spectra together with fitting lines are shown in Figure 4b. The EXAFS-derived structural parameters also indicated the existence of Ag–Ag bonds (Table S1). However, the Ag coordination number decreased from 8.1 to 2.1 with the increase of the exposure time from 24 to 72 h, and meanwhile Ag–S and Ag–O bonds appeared (Table S1), validating the results of XANES.

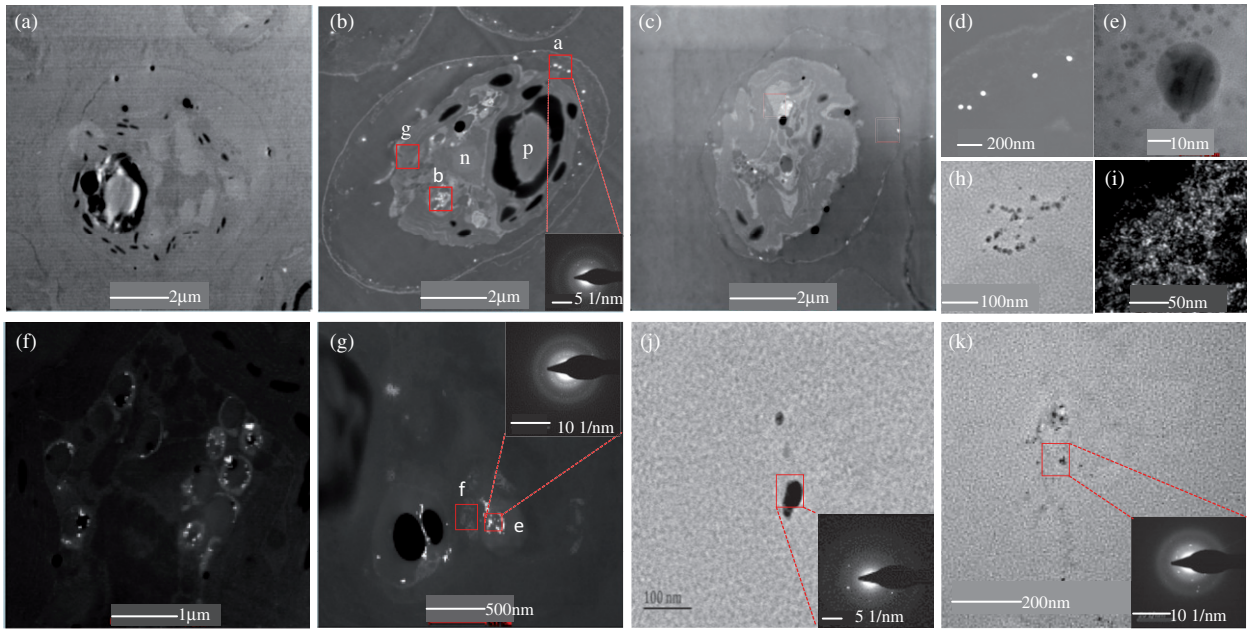

Figure 3. Distribution and physicochemical characterization of Ag in *C. reinhardtii* after exposure to CK (a), AgNPs (b) and Ag^+ (c). (d and e) Location of periplasmic space of AgNP-treated algae, area a in figure b. (f and g) Location in the cytoplasm of AgNP-treated algae, area b in figure b, (h) Area e in figure g. (i) Area f in figure g. (j) Location of periplasmic space of Ag^+-treated algae, area c in figure c. (k) Location in the cytoplasm of Ag^+-treated algae. (e and h) BF-TEM images. n, nucleus; p, pyrenoid.

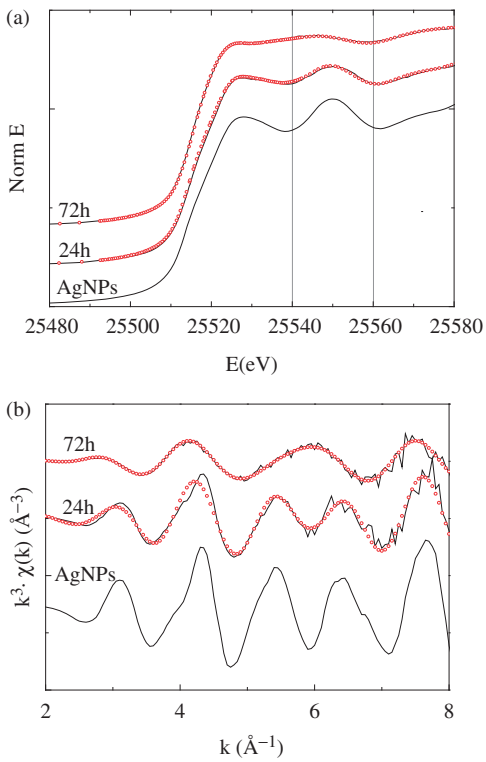

Figure 4. Synchrotron-based XAS analysis of silver speciation after AgNP interaction with *C. reinhardtii*. (a) Experimental XANES spectra (blank solid lines) and LCFs (red circles). (b) Experimental EXAFS spectra (black solid lines) and Levenberg–Marquardt nonlinear least squares fittings (red circles).

Discussion

Accurately elucidating cellular internalization of AgNPs is still a challenge due to the difficulties in visualizing their distribution inside cells with high spatial resolution. In this study, we applied a combination of high resolution imaging and in situ detection spectroscopic techniques to investigate the uptake, distribution and morphology of Ag in algae after exposure to AgNPs. The observations with NanoSIMS, HAADF-STEM, EDS and SAED collectively confirmed the existence of AgNPs inside the cells of *C. reinhardtii*. The accumulation of Ag was first observed in the periplasmic space and cytoplasm of the algae with NanoSIMS and EDS (Figure 2 and Figure S5a). Silver in the periplasmic space was identified as particles with the diameter of 10–20 nm via HAADF-STEM analysis (Figure 3d), which were further confirmed to be silver crystals (inset in Figure 3b) using SAED crystalline structure analysis (inset in Figure 3b). Silver in the cytoplasm was observed to coexist with sulfur both in particles with the diameter of 10–20 nm and in an amorphous form (area a in Figure 2, Figure S6b and Figures 3h and 3i), which were further identified as β-Ag_2S and silver thiolates by SAED and XAS analyses, respectively (inset in Figure 3g, Figure 4).

The presence of AgNPs in the periplasmic space suggested their entrance into algal cells by cellular internalization. However, besides the potential route of direct cellular internalization, it has been reported that Ag^+ ion released from AgNPs can be further reduced by living cells or extracellular polymeric substances to form AgNPs (Kang et al., 2014). In order to elucidate this issue, a comparative observation was conducted on the algae exposed to AgNPs and Ag^+. Although Ag was also found as particles in the periplasmic space of the algae after exposure to Ag^+, their detailed crystal structure was completely different from that of silver crystals arising from exposure to AgNPs (insets in Figure 3j and 3b). This excluded the possibility of the formation of AgNPs from Ag^+ ion in the periplasmic space of cells. By contrast, Ag particles were detected as β-Ag_2S in the cytoplasm of the algae and there was no essential difference between the algae exposed to AgNPs versus those exposed to Ag^+. So, it was very likely that the Ag_2S particles in the cytoplasm were formed from Ag^+ ion released from AgNPs. Furthermore, we did not observe AgNPs inside the vesicle or the endosome around the cell membrane or on the way to the endomembrane system, suggesting that there was no endocytosis or passive diffusion of AgNPs into the cytoplasm. Therefore, our observations were in favor of the view

that accumulation of Ag inside the cytoplasm of the algae could be attributed to the uptake of Ag^+ ion released from AgNPs followed by sulfidation, consistent with the conclusions of previous studies (Leclerc & Wilkinson, 2014; Ribeiro et al., 2015).

It must be noted that the released Ag^+ ion was sequestered into distinct subcellular compartments after entering the cytoplasm (Figures 3f and S6b). The membranous and hollow structure of the compartments resembles vacuoles that can serve as storage sites for excessive metals (Conn and Gilliham, 2010). This is an adaptive mechanism for algae to mitigate exposure toxicity (Choppala et al., 2014; Tian et al., 2011). Another mechanism for reducing toxicity was sulfidation of the released Ag^+ ion in the cytoplasm by sulfide precipitation and complexation with thiols from abundant molecules such as phytochelatins. This is the widely accepted mechanism for the complexation and sequestration of toxic heavy metals in plants (Chen et al., 2013a; Pal & Rai, 2010; Tian et al., 2011). In recent studies, the AgNP sulfidation products β-Ag_2S and silver thiolates were found in aquatic animals and human cells by using XAS analysis (Auffan et al., 2014; Hsiao et al., 2015; Wang et al., 2014). However, XAS analysis can only detect these products in bulk samples, and evidence for the presence of these sulfidation products at the cellular level is lacking. In this study, we for the first time, using NanoSIMS (Figure 2) and HAADF-STEM (Figure 3), identified their formation inside the cytoplasm, but no sulfidation of AgNPs outside the cytoplasm. This could be explained by the fact that there were few sulfides or thiols outside the cytoplasm, and that sulfidation of AgNPs with thiols is much more difficult than that of Ag^+ (Chen et al., 2013b). XAS analysis showed a great increase in the proportion of silver thiolates and silver sulfides with the increase of exposure time (from <30% in 24 h to 85% in 72 h), suggesting that there were large amounts of AgNPs entering the cytoplasm through the release of Ag^+ ion and then sulfidation, different from the results by Piccapietra et al. (2012), likely because of their short exposure time (1 h). It has been accepted that the dissolution rate of AgNPs is proportional to the particle size; therefore, it is reasonable to expect that both the uptake and transformation of AgNPs by algae is much easier than for bulk silver.

Conclusions

In this study, internalization of AgNPs by *C. reinhardtii* was for the first time evidenced by a combination of high resolution imaging techniques. Observations suggested that AgNPs would enter the periplasmic space after cellular internalization into cells of *C. reinhardtii*. Sulfidation of Ag^+ ion released from AgNPs by thiolates and sulfides led to an increasing sequestration of Ag in the cytoplasm of algae. It is still difficult to employ a single technique to elucidate the uptake and behaviors of nanoparticles inside cells. Thus, the endeavor of this study combining NanoSIMS, HAADF-TEM and XAS to investigate these processes provides a valuable reference for understanding the interactions of nanoparticles with cells and bio-macromolecules. This study provides sufficient evidence for cellular internalization and biotransformation of AgNPs in *C. reinhardtii*, which is very helpful for understanding the behavior and fate of AgNPs in the aquatic environment.

Acknowledgments

We are grateful to Dr. Jun Weng and Fei Shi for their advice on sample preparation for NanoSIMS analysis and François Horréard, François Hillion and Adina Lazar from CAMECA, France for their generous support in the NanoSIMS detection and data analysis. We thank the Shanghai Synchrotron Radiation facility for the provision of synchrotron beam time under award 13SRBL14W16825.

Declaration of interest

The authors report no conflicts of interest and are responsible for the content and writing of the paper. Financial supports were provided by the Strategic Priority Research Program of the Chinese Academy of Sciences (Grant XDB14020202) and the National Natural Science Foundation of China (Projects 21321004 and 21277154) .

References

Auffan M, Matson CW, Rose J, Arnold M, Proux O, Fayard B, et al. 2014. Salinity-dependent silver nanoparticle uptake and transformation by Atlantic killifish (*Fundulus heteroclitus*) embryos. Nanotoxicology 8: 167–76.

Behra R, Sigg L, Clift MJ, Herzog F, Minghetti M, Johnston B, et al. 2013. Bioavailability of silver nanoparticles and ions: from a chemical and biochemical perspective. J R Soc Interface 10:20130396.

Chen S, Goode AE, Sweeney S, Theodorou IG, Thorley AJ, Ruenraroengsak P, et al. 2013a. Sulfidation of silver nanowires inside human alveolar epithelial cells: a potential detoxification mechanism. Nanoscale 5:9839–47.

Chen S, Theodorou IG, Goode AE, Gow A, Schwander S, Zhang JF, et al. 2013b. High-resolution analytical electron microscopy reveals cell culture media-induced changes to the chemistry of silver nanowires. Environ Sci Technol 47:13813–21.

Choppala G, Saifullah, Bolan N, Bibi S, Iqbal M, Rengel Z, et al. 2014. Cellular mechanisms in higher plants governing tolerance to cadmium toxicity. Crit Rev Plant Sci 33:374–91.

Conn S, Gilliham M. 2010. Comparative physiology of elemental distributions in plants. Ann Bot 105:1081–102.

Cronholm P, Karlsson HL, Hedberg J, Lowe TA, Winnberg L, Elihn K, et al. 2013. Intracellular uptake and toxicity of Ag and CuO nanoparticles: a comparison between nanoparticles and their corresponding metal ions. Small 9:970–82.

Das P, Metcalfe CD, Xenopoulos MA. 2014. Interactive effects of silver nanoparticles and phosphorus on phytoplankton growth in natural waters. Environ Sci Technol 48:4573–80.

Fabrega J, Luoma SN, Tyler CR, Galloway TS, Lead JR. 2011. Silver nanoparticles: behaviour and effects in the aquatic environment. Environ Int 37:517–31.

Garcia CP, Burchardt AD, Carvalho RN, Gilliland D, Antonio DC, Rossi F, Lettieri T. 2014. Detection of silver nanoparticles inside marine diatom *Thalassiosira pseudonana* by electron microscopy and focused ion beam. PLoS One 9:e96078.

Harris EH. (2009). The Chlamydomonas Sourcebook. Oxford, UK: Elsevier Inc.

Hedberg J, Skoglund S, Karlsson ME, Wold S, Wallinder IO, Hedberg Y. 2014. Sequential studies of silver released from silver nanoparticles in aqueous media simulating sweat, laundry detergent solutions and surface water. Environ Sci Technol 48:7314–22.

Hong-Hermesdorf A, Miethke M, Gallaher SD, Kropat J, Dodani SC, Chan J, et al. 2014. Subcellular metal imaging identifies dynamic sites of Cu accumulation in *Chlamydomonas*. Nat Chem Biol 10:1034–42.

Hsiao IL, Hsieh YK, Wang CF, Chen IC, Huang YJ. 2015. Trojan-horse mechanism in the cellular uptake of silver nanoparticles verified by direct intra- and extracellular silver speciation analysis. Environ Sci Technol 49:3813–21.

Jimenez-Lamana J, Laborda F, Bolea E, Abad-Alvaro I, Castillo JR, Bianga J, et al. 2014. An insight into silver nanoparticles bioavailability in rats. Metallomics 6:2242–9.

Kang F, Alvarez PJ, Zhu D. 2014. Microbial extracellular polymeric substances reduce Ag^+ to silver nanoparticles and antagonize bactericidal activity. Environ Sci Technol 48:316–22.

Kim B, Park CS, Murayama M, Hochella MF. 2010. Discovery and characterization of silver sulfide nanoparticles in final sewage sludge products. Environ Sci Technol 44:7509–14.

Leclerc S, Wilkinson KJ. 2014. Bioaccumulation of Nanosilver by *Chlamydomonas reinhardtii* – nanoparticle or the free ion? Environ Sci Technol 48:358–64.

Levard C, Hotze EM, Lowry GV, Brown GE. 2012. Environmental transformations of silver nanoparticles: impact on stability and toxicity. Environ Sci Technol 46:6900–14.

Liu J, Wang Z, Liu FD, Kane AB, Hurt RH. 2012. Chemical transformations of nanosilver in biological environments. ACS Nano 6:9887–99.

Lowry GV, Espinasse BP, Badireddy AR, Richardson CJ, Reinsch BC, Bryant LD, et al. 2012. Long-term transformation and fate of manufactured Ag nanoparticles in a simulated large scale freshwater emergent wetland. Environ Sci Technol 46:7027–36.

Miao AJ, Luo Z, Chen CS, Chin WC, Santschi PH, Quigg A. 2010. Intracellular uptake: a possible mechanism for silver engineered nanoparticle toxicity to a freshwater alga *Ochromonas danica*. PLoS One 5:e15196.

Mitrano DM, Rimmele E, Wichser A, Erni R, Height M, Nowack B. 2014. Presence of nanoparticles in wash water from conventional silver and nano-silver textiles. ACS Nano 8:7208–19.

Moore KL, Chen Y, Van De Meene AM, Hughes L, Liu W, Geraki T, et al. 2014. Combined NanoSIMS and synchrotron X-ray fluorescence reveal distinct cellular and subcellular distribution patterns of trace elements in rice tissues. New Phytol 201:104–15.

Navarro E, Wagner B, Odzak N, Sigg L, Behra R. 2015. Effects of differently coated silver nanoparticles on the photosynthesis of *Chlamydomonas reinhardtii*. Environ Sci Technol 49:8041–7.

Pal R, Rai JP. 2010. Phytochelatins: peptides involved in heavy metal detoxification. Appl Biochem Biotechnol 160:945–63.

Piccapietra F, Allue CG, Sigg L, Behra R. 2012. Intracellular silver accumulation in *Chlamydomonas reinhardtii* upon exposure to carbonate coated silver nanoparticles and silver nitrate. Environ Sci Technol 46:7390–7.

Pratsinis A, Hervella P, Leroux JC, Pratsinis SE, Sotiriou GA. 2013. Toxicity of silver nanoparticles in macrophages. Small 9:2576–84.

Ribeiro F, Gallego-Urrea JA, Goodhead RM, Van Gestel CA, Moger J, Soares AM, Loureiro S. 2015. Uptake and elimination kinetics of silver nanoparticles and silver nitrate by *Raphidocelis subcapitata*: the influence of silver behaviour in solution. Nanotoxicology 9:686–95.

Sadanaga R, Sueno S. 1967. X-ray study on the alpha–beta transition of Ag_2O. Mineral J (Japan) 5:124–8.

Sekine R, Khaksar M, Brunetti G, Donner E, Scheckel KG, Lombi E, Vasilev K. 2013. Surface immobilization of engineered nanomaterials for in situ study of their environmental transformations and fate. Environ Sci Technol 47:9308–16.

Seltenrich N. 2013. Nanosilver: weighing the risks and benefits. Environ Health Perspect 121:A220–5.

Sharma VK, Siskova KM, Zboril R, Gardea-Torresdey JL. 2014. Organic-coated silver nanoparticles in biological and environmental conditions: fate, stability and toxicity. Adv Colloid Interface Sci 204:15–34.

Sorensen SN, Baun A. 2015. Controlling silver nanoparticle exposure in algal toxicity testing A matter of timing. Nanotoxicology 9:201–9.

Thorley AJ, Ruenraroengsak P, Potter TE, Tetley TD. 2014. Critical determinants of uptake and translocation of nanoparticles by the human pulmonary alveolar epithelium. ACS Nano 8:11778–89.

Tian S, Lu L, Labavitch J, Yang X, He Z, Hu H, et al. 2011. Cellular sequestration of cadmium in the hyperaccumulator plant species *Sedum alfredii*. Plant Physiol 157:1914–25.

Tulve NS, Stefaniak AB, Vance ME, Rogers K, Mwilu S, Lebouf RF, et al. 2015. Characterization of silver nanoparticles in selected consumer products and its relevance for predicting children's potential exposures. Int J Hyg Environ Health 218:345–57.

Von Moos N, Bowen P, Slaveykova VI. 2014. Bioavailability of inorganic nanoparticles to planktonic bacteria and aquatic microalgae in freshwater. Environ Sci Nano 1:214–32.

Wang HH, Ho KT, Scheckel KG, Wu FC, Cantwell MG, Katz DR, et al. 2014. Toxicity, bioaccumulation, and biotransformation of silver nanoparticles in marine organisms. Environ Sci Technol 48: 13711–17.

Wang LM, Zhang TL, Li PY, Huang WX, Tang JL, Wang PY, et al. 2015. Use of synchrotron radiation-analytical techniques to reveal chemical origin of silver-nanoparticle cytotoxicity. ACS Nano 9: 6532–47.

Wyckoff RWG. 1963. Crystal Structures. 2nd ed. Vol. 1. New York: Interscience Publishers, 77.

Yang X, Jiang C, Hsu-Kim H, Badireddy AR, Dykstra M, Wiesner M, et al. 2014. Silver nanoparticle behavior, uptake, and toxicity in *Caenorhabditis elegans*: effects of natural organic matter. Environ Sci Technol 48:3486–95.

Supplementary material available online

Supplementary Table S1 and Figures S1–S8